Hindawi
Journal of Nanomaterials
Volume 2021, Article ID 6679637, 14 pages
https://doi.org/10.1155/2021/6679637

Research Article

Gamma Irradiation-Assisted Synthesis of Silver Nanoparticle-Embedded Graphene Oxide-TiO_2 Nanotube Nanocomposite for Organic Dye Photodegradation

Duy Khang Nguyen Vu[1] **and Dang Khoa Vo Nguyen**[1,2]

[1]*Institute of Applied Materials Science-Vietnam Academy of Science and Technology, 01A TL29 Street, Thanh Loc Ward, District 12, Ho Chi Minh City 70000, Vietnam*
[2]*Graduate University of Science and Technology-Vietnam Academy of Science and Technology, 18 Hoang Quoc Viet Street, Nghia Do Ward, Cau Giay District, Ha Noi 10000, Vietnam*

Correspondence should be addressed to Dang Khoa Vo Nguyen; vndkhoa@iams.vast.vn

Received 23 October 2020; Revised 1 January 2021; Accepted 8 January 2021; Published 25 January 2021

Academic Editor: Zhi Li Xiao

In this work, silver nanoparticle- (AgNP-) embedded graphene oxide- (GO-) TiO_2 nanotube (TNT) nanocomposite (labelled GAT) was successfully synthesized by gamma ray radiolysis. The influence of irradiation process, including one-step and two-step assistances and at different irradiation doses (5, 10, 15, 20, and 25 kGy), on the GAT's physicochemical properties was achieved. Structure and properties of irradiated materials were analyzed by Fourier-transformed infrared (FT-IR), ultraviolet-visible absorption (UV-Vis), and Raman spectroscopies; X-ray diffraction (XRD); and scanning electron (SEM) and transmission electron (TEM) microscopies. In addition, selective scavengers of e^-_{aq} and ·OH radicals were used to investigate the radiolytic synthesis of GAT nanocomposite. It was revealed that gamma ray irradiation could strongly support the relation of the composite synthesis. Furthermore, the synthesized GAT nanocomposites showed a significant effect for Rhodamine B (RhB) photodecomposition after 60 minutes of natural sunlight exposure and evaluation by UV-Vis absorption spectroscopy. Briefly, the obtained results highlighted the potential of gamma irradiation as a "clean" and controllable way for synthesizing beneficial nanocomposite materials for wastewater purification and other environmental aspects.

1. Introduction

Gamma ray irradiation is among the physical methods widely applied for the synthesis of different sorts of metallic nanoparticles [1–3]. During the exposure to gamma ray, water radiolysis occurs, releasing hydrated electrons (e^-_{aq}) and hydrogen atoms ($H^·$), which are capable of reducing metal cations to zero-valent clusters (Figure 1) [4, 5]. In comparison with chemical, electrochemical, or physical synthetic processes, such method for producing metal nanoparticles can proceed without further steps of purification, due to the lack of byproducts and pollutants. In addition, gamma ray irradiation was demonstrated to be controllable, hence its conformability for instantaneous and homogenous synthesis of metallic nanoparticles [2]. The ability of radiolyzing molecules and releasing charged moieties also result in the application of gamma ray irradiation in the synthesis of many other hybrid nanomaterials [3, 6], to overcome shortcomings, elevate the advantages of each component, and expand their applications. Gamma ray irradiation-assisted synthesis of different types of materials (zeolite [7], thin films [8, 9], minerals [10], hydrogels [11], membranes [12], as well as many others [13, 14]) have been studied, which reinforced the high potential of this technique to be widely applied in advanced materials synthesis.

Isopropanol (i-PrOH) is well known for its ability of capturing radicals in reaction solutions, by means of the interaction between its alcohol group and the radical [15], as illustrated in Scheme 1. This radical scavenger has been applied in many publications regarding radiation process

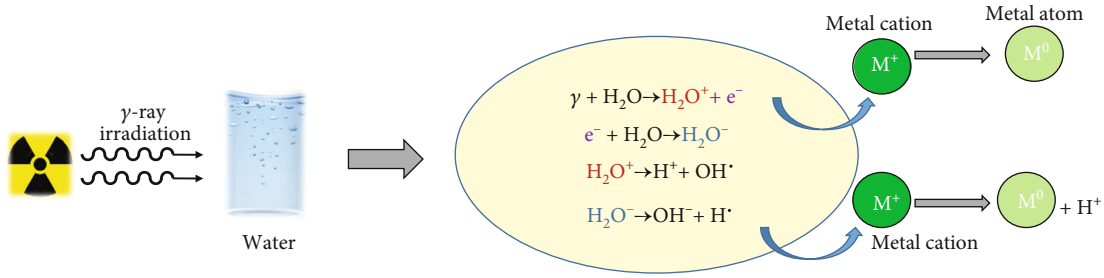

Figure 1: Water radiolysis and metal atom formation induced by gamma irradiation.

$$H_3C{-}CHOH{-}CH_3 + {\bullet}OH \rightarrow H_2O + {\bullet}CH_2{-}CHOH{-}CH_3$$

$$N_2O + e^-_{aq} \rightarrow N_2 + O^-$$

Scheme 1: The hydroxyl radical and hydrated electron scavenging of i-PrOH and N_2O.

(laser [15], gamma [4], or electron beam [16]), clarifying the way in which the target material was affected. Nitrous oxide (N_2O) was revealed to be capable of capturing hydrated electrons [17] (Scheme 1), and it has then been used in many studies, especially in the radiative and catalytic aspects, for radiation and catalytic mechanism determination. These two scavengers, therefore, could be applied in our investigation of gamma irradiation's effects on nanocomposite synthesis with high conformability.

Renowned as the "oxidized form" of graphene, graphene oxide (GO) is similar in the layer structure, but with various oxygen-bearing functional groups such as carbonyls (−C=O), carboxyls (−COOH), and alcohols (C − OH) on the surface [18]. Among graphene-based materials, graphene oxide was noticeable for the ability of immobilizing metal oxides (TiO_2 [19, 20]) and many other chemicals (such as glucose oxidase (GOD) or bilirubin oxidase (BOD) [21]), thanks to the stable chemical bonds between oxygen atoms in its functional groups and metal oxides. Hybrid nanomaterials composed of GO and TiO_2 nanoforms (such as nanoparticles or nanotubes) were synthesized successfully and exhibited fascinating photocatalytic activity [22, 23].

Titanium dioxide (TiO_2) has been attracting scientific interests due to its spectacular activity on photodegrading contaminants from the environment. Its ability of photodecomposing pollutants, especially organic dyes such as rhodamine B, methylene blue, or crystal violet, has been ameliorated by modification in many sides: forms (nanoparticles to nanotubes [24, 25] or nanowires [26]), composition (metals and metal oxide doping [27, 28], organodoping [29]), and structure optimization [30]. TiO_2 nanotubes have been demonstrated possessing higher specific surface area, with an orderly one-dimensional structure, comparing with nanoparticles, providing great contribution to its photocatalytic activity. Combination of TiO_2 nanotubes [31] or nanotube arrays [32] with reduced graphene oxide by gamma ray irradiation, as well as many others [33–35], has been published.

Among the highly potential nanomaterials for combining with TiO_2 and GO, silver nanoparticles (AgNPs) emerged as a reasonable choice due to their fascinating conductivity, catalytic properties, and antibacterial activity. AgNPs have been picked as ideal metallic nanoparticles for decorating on many kinds of surfaces: wires [36], gels [37], or sheets [38]. Such assemblage enhanced the properties of precursory materials and expanded significantly their applications.

Over 50 billion tons of chemicals, especially organic dyes, are used annually in dyeing procedures, of which approximately 20% is discharged into aqueous effluent without any treatments [39]. The existence of such pollutants in wastewater is no doubt an obstinate menace to not only aquatic and terrestrial ecosystems but also human health. It has been revealed recently that some organic compounds commonly used in the dyeing process such as bisphenol A (BPA) or bisphenol S (BPS) can cause endocrine disruption [39]. It is, therefore, exigent for scientific studies to seek solutions for contaminant elimination in wastewater.

Chemical [40] or electrochemical [41, 42] pathways were applied in the combination of silver nanoparticles, TiO_2 nanotubes, and graphene-based materials. In such publications, reduced graphene oxide was used as the "support" for these nanomaterials. In this work, we aim to apply gamma ray irradiation, a "clean" and controllable method, for the synthesis of silver nanoparticle-embedded graphene oxide-TiO_2 nanotube nanocomposite (denoted as GAT), with the high expectation of combining advantages of each component, especially photocatalytic activity (Figure 2). Rhodamine B (RhB), one of the most important and widely used organic dyes, was used as the target and its photodecomposition was conducted under natural sunlight exposure. In order to obtain a profound evaluation of gamma ray's effect on the formation of GAT nanocomposite, the dose range was altered and two different irradiation assistances (one step and two step) were applied.

2. Experimental

2.1. Reagents. Graphite powder was purchased from Acros Organics (Germany); silver nitrate and TiO_2 anatase nanopowders were purchased from Merck (Germany). RhB dye was purchased from HiMedia, India. Other chemicals were in analytical pure grade, and deionized water was used throughout the work.

2.2. Synthesis of Graphene Oxide (GO), Silver Nanoparticles (AgNPs), and TiO_2 Nanotubes (TNTs). GO sheets were synthesized following the route published by Marcano et al. [43], using graphite powder as precursor and potassium

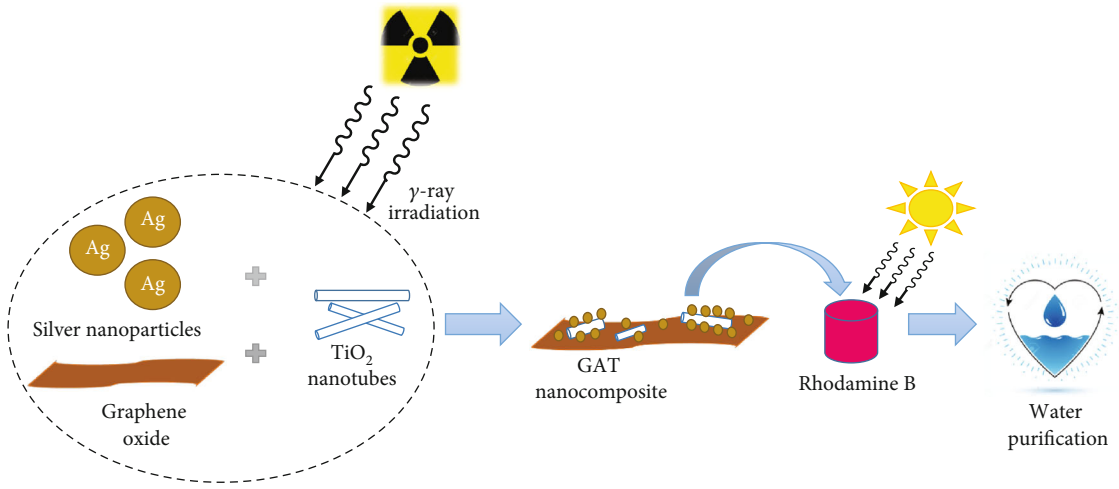

Figure 2: The idea of creating GAT nanocomposite for rhodamine B photodecomposition.

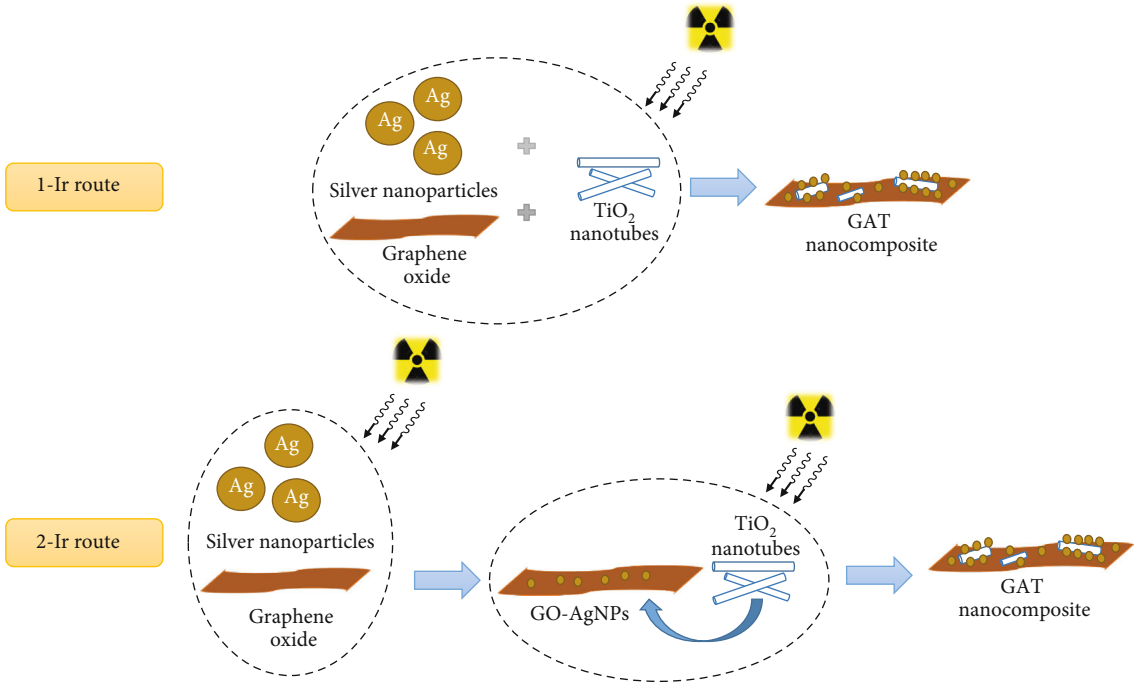

Figure 3: Schematic description of two manners of gamma irradiation for GAT synthesis.

permanganate as oxidizer. The product was vacuum dried for further synthesis. AgNPs were obtained by the reduction of silver nitrate solution using sodium borohydride, following the process published by Aherne et al. [44] Polyethylene glycol (PEG) was used as the substitute for poly(sodium styrene sulfonate) (PSSS). The product solution was sealed and kept in the dark for further procedure. Thirdly, TNTs were synthesized following the method published by Zavala and Ávila-Santos [45], using the TiO_2 anatase nanopowder as a titania precursor. The product was vacuum dried to obtain the powder form.

2.3. Synthesis of Graphene Oxide-Silver Nanoparticles-TiO_2 Nanotube Nanocomposite (GAT) and Gamma Ray's Effect Investigation. For the profound investigation on gamma irradiation's effects on the synthesis of GAT nanocomposites, in this work, two different gamma ray irradiation assistances were applied, as illustrated in Figure 3, the one-step and the two-step assistances, abbreviated as 1-Ir route and 2-Ir route, respectively.

In the 1-Ir route, obtained GO and TNTs were dispersed separately in a PEG 0.5 g L^{-1} aqueous solution by sonication in 30 minutes and then mixed with each other. The mixture was joined by AgNP solution and followed by another 30 minutes of sonication. The GO-AgNPs-TNTs mixture was then gamma ray irradiated by a COBALT-60/B irradiator, at dose ranges of 5, 10, 15, 20, and 25 kGy. The products were labelled GAT-1-Ir-5, GAT-1-Ir-10, GAT-1-Ir-15, GAT-1-Ir-20, and GAT-1-Ir-25, respectively.

In the 2-Ir route, obtained GO product was dispersed in a PEG 0.5 g L^{-1} aqueous solution by sonication in 30 minutes. The solution was then joined by AgNP solution and followed by another 30 minutes of sonication. The GO-AgNP mixture was then gamma ray irradiated by a COBALT-60/B irradiator, at dose ranges of 5, 10, 15, 20, and 25 kGy. During the irradiation process, the solution of TNTs dispersed in PEG 0.5 g L^{-1} by 30 minutes of sonication was prepared. After the irradiation finished, the TNT solution was added instantaneously into the GO-AgNP solution and the mixture was followed by another irradiation, with dose range remained unchanged. The products were labelled GAT-2-Ir-5, GAT-2-Ir-10, GAT-2-Ir-15, GAT-2-Ir-20, and GAT-2-Ir-25, respectively.

In addition to the variation in irradiation dose and assistance, effect of gamma ray on the combination of GO, AgNPs, and TNTs was investigated by means of irradiation with the presence of isopropanol (i-PrOH), a radical scavenger [46], and nitrous oxide (N_2O), an electron capturer [47]. The process of GAT preparation and irradiation followed the 1-Ir route, with i-PrOH as the substitute for PEG solution. For the N_2O case, prior to gamma ray irradiation, GAT solutions were scoured with N_2O for 5 minutes, whereas all other steps remained constant. The products were labelled GAT-I-5, GAT-I-10, GAT-I-15, GAT-I-20, and GAT-I-25 for isopropanol and GAT-1-N-5, GAT-1-N-10, GAT-1-N-15, GAT-1-N-20, and GAT-1-N-25 for N_2O.

Gamma irradiations were performed at VINAGAMMA Center (Ho Chi Minh City, Vietnam) on a ^{60}Co source with the dose rate of 1.3 kGy h^{-1} measured by the ethanol–chlorobenzene dosimetry system (ISO/ASTM 51538-2002(E)). The irradiating duration was 4 hours, 8 hours, 12 hours, 16 hours, and 20 hours for the 5 kGy, 10 kGy, 15 kGy, 20 kGy, and 25 kGy, respectively. After irradiation, all samples were stored in ambient temperature for further characterization.

2.4. Material Characterization and Conditions. All obtained products were characterized using spectroscopic and microscopic methods: Fourier-transformed infrared (FT-IR), UV-Vis adsorption (UV-Vis), Raman, X-ray diffraction (XRD), scanning electron (SEM), and transmission electron (TEM). FT-IR spectra were recorded on a MIR/NIR Frontier (PerkinElmer, USA) spectrometer, with the wavenumber range of 4000-400 cm^{-1}, KBr pellets with 5 mg of sample for each GAT nanocomposite. The average scanning speed was 30 scans/min. For UV-Vis absorption spectra recording, an UV-1800 (Shimadzu, Japan) spectrometer was used, with the interval of 0.1 nm and the scanning speed of 50 nm/min. Raman spectra were recorded on an XploraOne (Horiba, Japan) spectrometer, with the laser wavelength of 532 nm and grating of 900 gr/mm. X-ray diffractograms were obtained by using a D2 Phaser (Bruker, Germany) diffractometer with Cu/Kα as the X-ray source and at scanning speed of 0.5 degree/min. For SEM and TEM imaging, a FE-SEM S-4800 (Hitachi, Japan) and JEOL JEM-1400 (JEOL, USA) microscopes were used.

2.5. Rhodamine B Photodecomposition. Synthesized GAT nanocomposites were followed by the photodecomposition of RhB dye under natural sunlight exposure, based on the procedure published by Nagaraja et al. [48] Specifically, GAT samples were dispersed in a glass flask containing 20 mL of 10 ppm RhB solution and stirred in the dark for 15 min so that the absorption equilibrium was established. The solutions were then continuously stirred for 60 min under natural sunlight irradiation. The photocatalytic reactions were conducted from 11 a.m. to 12 p.m., at which the sunlight's intensity was the most stable. After 60 min, the solutions were isolated from the sunlight, filtered to eliminate all remaining catalyst particles, and evaluated by UV-Vis absorption spectroscopy.

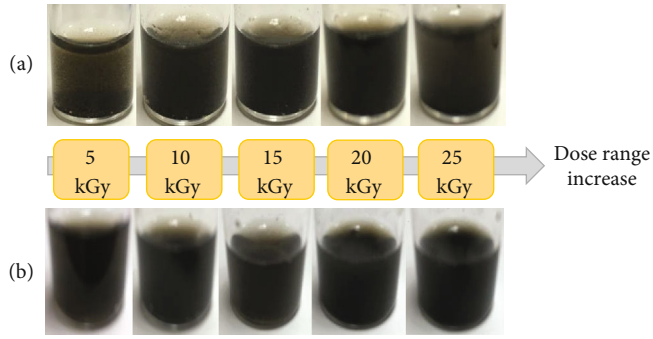

Figure 4: Synthesized GAT solutions ((a) 1-Ir route and (b) 2-Ir route) at different irradiation doses.

Before the photodecomposition evaluation, a 10 ppm RhB aqueous solution was prepared and performed UV-Vis absorption in order to determine the specific adsorbent wavelength. This wavelength was applied for RhB's standard curve establishment, with the RhB concentrations as 0, 2, 4, 6, 8, and 10 ppm. The nanocomposites' ability of RhB photodecomposing was determined by means of their decoloration efficiency, or DE, value, which was calculated as in Eq. (1), where C_0 and C (ppm) is the dye's initial and postreaction concentrations.

$$\mathrm{DE}\,(\%) = [1 - (C/C_0)] \times 100. \quad (1)$$

Prior to the photodecomposition experiments, the proportion of GO, AgNPs, and TNTs in GAT samples was determined using inductively coupled plasma-mass spectroscopy (ICP-MS), on a NexION®2000 (PerkinElmer, USA) spectrometer. All samples were dissolved in hot HNO_3 65%/HF 10% solution to convert all components into soluble compounds and they were then evaluated by the ICP-MS spectrometer.

3. Results and Discussion

3.1. GAT Nanocomposite Characterization

3.1.1. Effect of Irradiation Doses and Assistance. Postirradiated GAT nanocomposites at different doses were obtained as dark brown solutions (Figure 4). There were no obvious differences in solutions' appearance between the 1-Ir and 2-Ir routes as the irradiation dose increased. The FT-IR spectra (Figure 5) exhibited characteristic signals: at ~3400 cm^{-1} (O – H groups), [49]~1620 cm^{-1} (C=C and Ti – OH bonds),

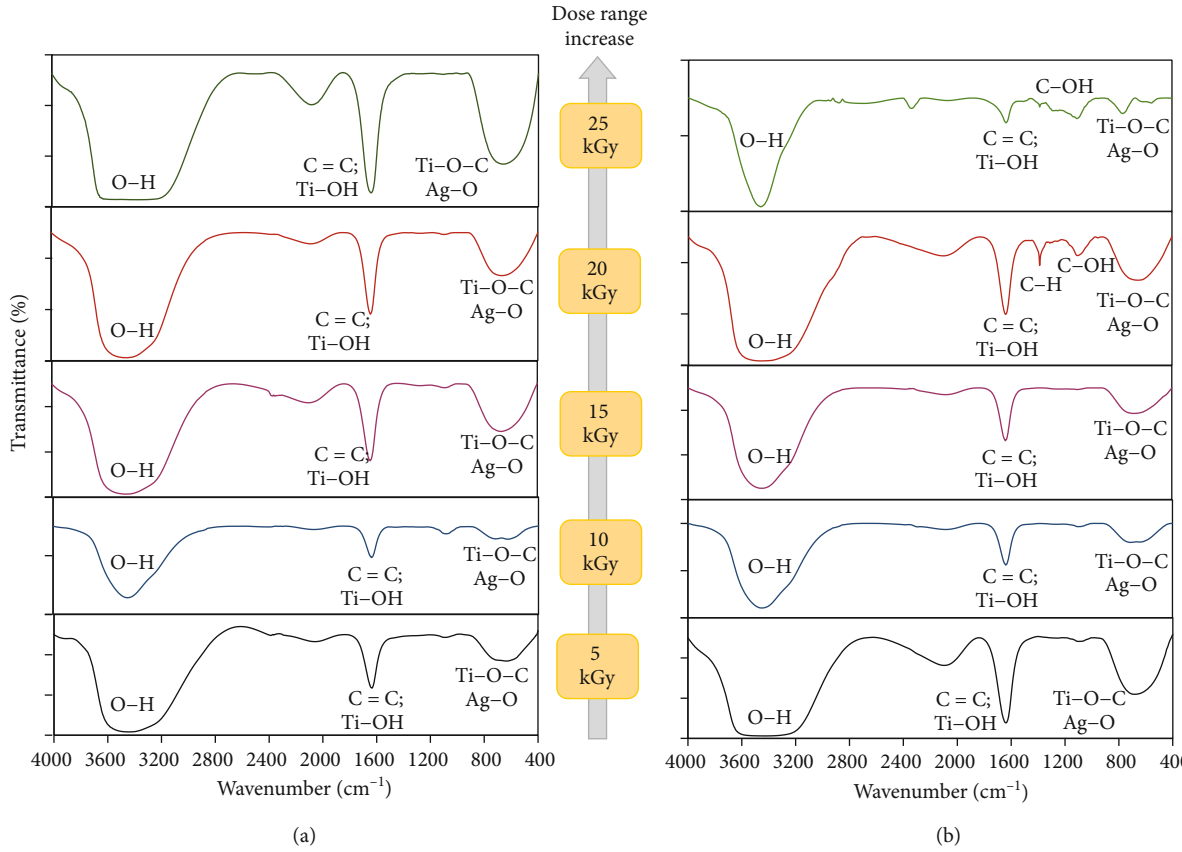

Figure 5: FT-IR spectra of GAT nanocomposites ((a) 1-Ir route and (b) 2-Ir route) at different irradiation doses.

[49, 50] and ~500-700 cm^{-1} (Ti – O – C and Ag – O bonds) [1, 51]. In the 1-Ir route samples, all signals became stronger as the dose augmented, indicating more chemical interaction among GO, AgNPs, and TNTs in the nanocomposites. Similar tendency was observed in the spectra of 2-Ir route samples at the dose ranges of 5, 10, and 15 kGy. Signals of C – H (−1350 cm^{-1}) and C – OH (~1100 cm^{-1}) bonds became more obvious and those of C=C bond diminished in the 20 kGy and 25 kGy 2-Ir route samples, indicating the possible partial reduction of highly oxidative functional groups of GO [52]. Moreover, signals of Ti – O – C and Ag – O bonds decreased in the 2-Ir route nanocomposite at the highest irradiation dose. It could be inferred from this result that the gamma ray overirradiation exhibited certain effects on the interaction among GO, AgNPs, and TNTs in GAT nanocomposites. Ti – O bond energy was much higher than that of Ag – O (776 kJ.mol^{-1} [53] and 220 kJ.mol^{-1} [54], respectively), hence its lower possibility of severing than Ag – O bond. Comparing with similar nanocomposites synthesized by nongamma routes [55] and the spectra of bare GO, TiO_2, and silver nanoparticles [51, 55], similarities in identical signals for each component in GAT nanocomposite were observed clearly, hence our consideration that gamma ray irradiation resulted in the bonding among GO, AgNPs, and TNTs to form nanocomposite product like other synthesis routes such as chemical reduction. It was noticeable in the FT-IR spectra that the signal of C=O bond (at ~1720 cm^{-1} [56]) was not observed clearly in all GAT samples, which resembled that of gamma ray-assisted reduced graphene oxide [56]. Three possibilities could be inferred from this result: the complete and direct reduction of GO to rGO induced by gamma ray irradiation, the conversion of the C=O bonds to the C – O – M ones (M : Ag or Ti), and the very few remaining C=O groups on GO's surface after interaction with AgNPs and TNTs. The presence of Ti – O – C and Ag – O bonds' signals led to our consideration that the second and third possibilities were more likely to occur during the exposure of GAT samples to gamma ray irradiation.

Chemical interaction among GO, AgNPs, and TNTs during gamma ray exposure was assured by the UV-Vis absorption spectra (Figure 6). In the 1-Ir route samples, as the irradiation dose increased, AgNPs' absorption peak at ~400 nm diminished and became absent at the highest dose. This result could be explained that the high irradiation dose induced the PEG molecule degradation, hence their loss of protective ability on silver nanoparticles [1, 57]. In addition, absorption signal of TNTs became more obvious as the dose augmented, indicating their higher crystallization. Comparison of obtained spectra of the nanocomposite with those of sole GO, AgNPs, and TNTs [1] led to our consideration that the TNT component in GAT nanocomposites was the most stable under gamma ray irradiation. For the 2-Ir route samples, at lower irradiation doses (5; 10 and 15 kGy), UV-Vis absorption spectra resembled those of 1-Ir route samples at high irradiation those (20 and 25 kGy), demonstrating the

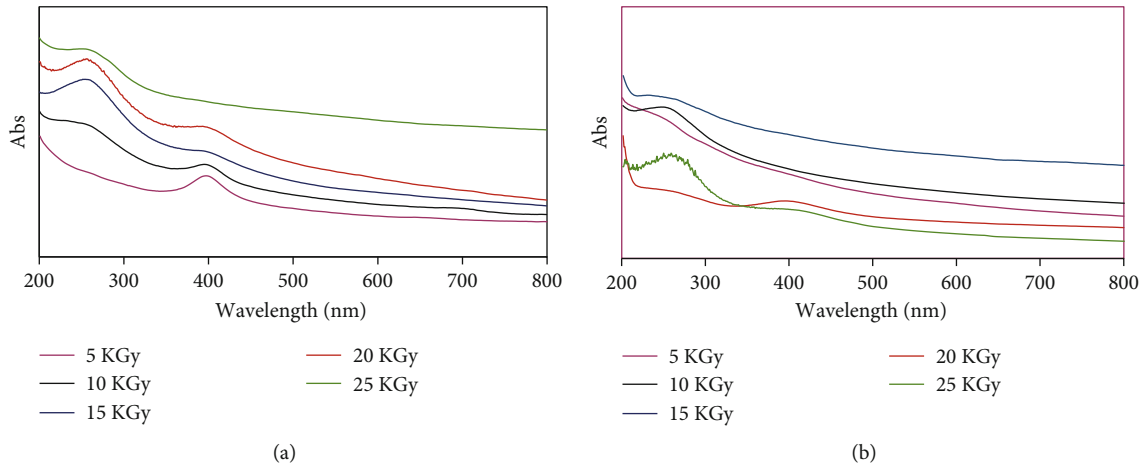

Figure 6: UV-Vis absorption spectra of GAT nanocomposites ((a) 1-Ir route and (b) 2-Ir route) at different irradiation doses.

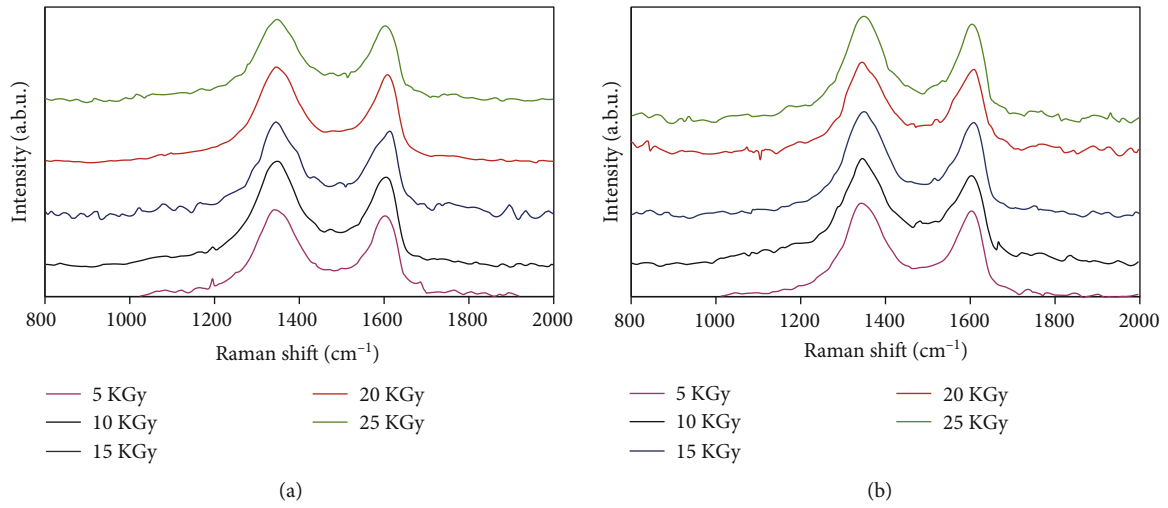

Figure 7: Raman spectra of GAT nanocomposites ((a) 1-Ir route and (b) 2-Ir route) at different irradiation doses.

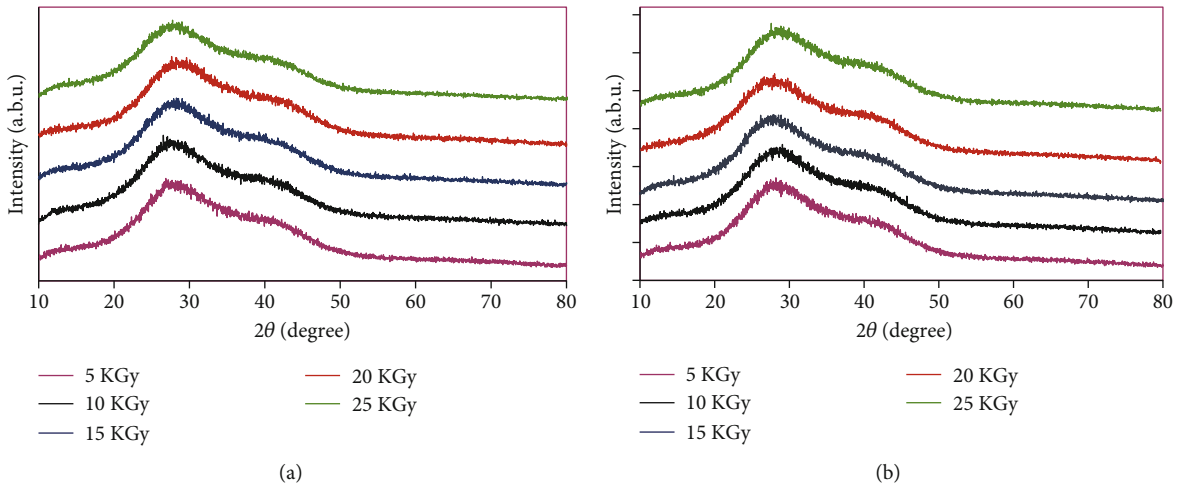

Figure 8: X-ray diffractogram of GAT nanocomposites ((a) 1-Ir route and (b) 2-Ir route) at different irradiation doses.

stronger "linking" effect of gamma ray on GAT nanocomposite during numerous times of irradiation. When the dose increased higher (20 and 25 kGy), TNTs' signals at ~255 nm became more similar to modified TNTs [58], indicating certain changes in the structure of this component. Thirdly, there were no obvious GO's signals in the spectra of all

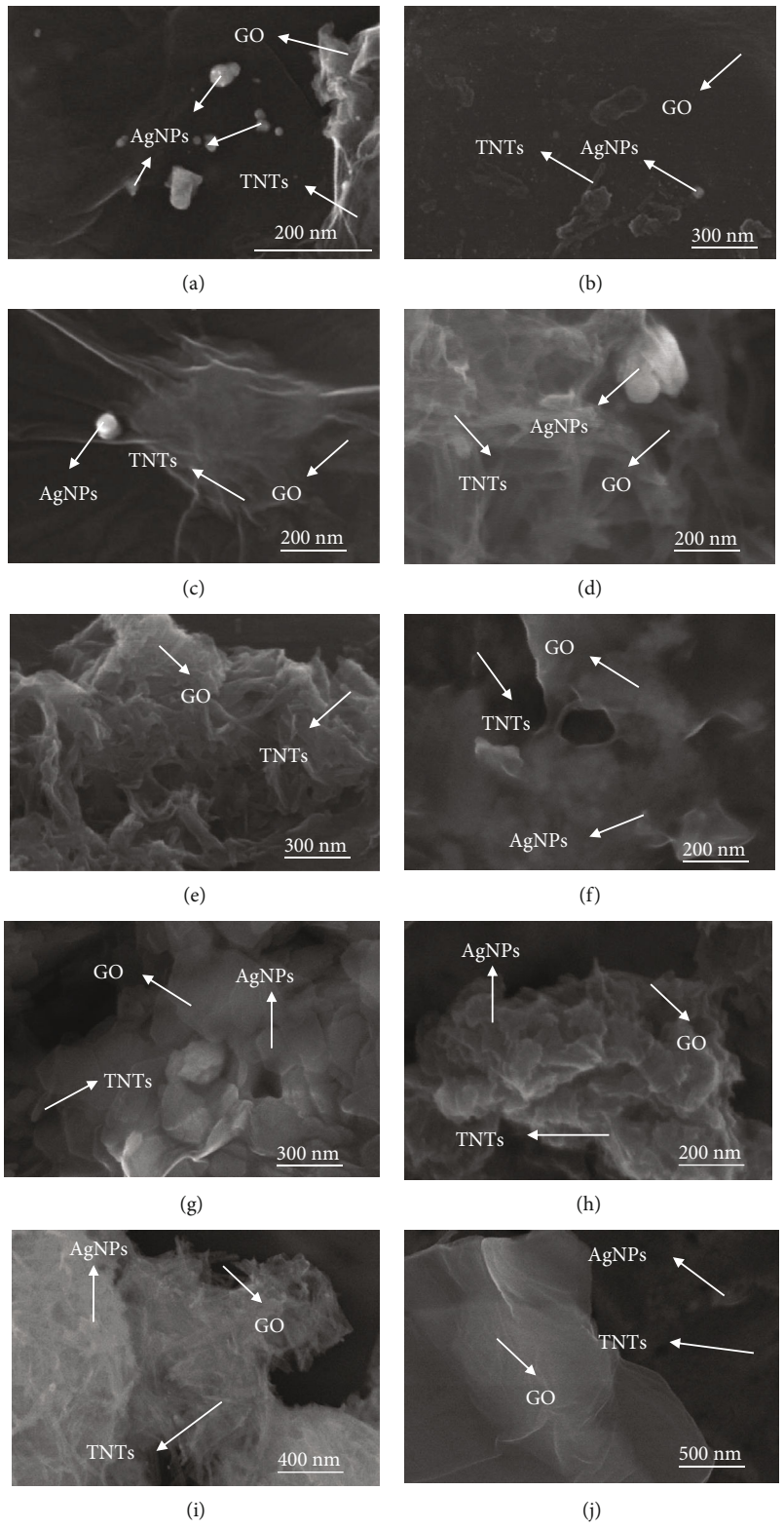

Figure 9: SEM images of 1-Ir route ((a–e) GAT-1-Ir-5 to GAT-1-Ir-25) and 2-Ir route ((f–j) GAT-2-Ir-5 to GAT-2-Ir-25) nanocomposites.

samples, of which possible explanation was its covering with TNTs and AgNPs on the surface [1, 51].

Raman spectra (Figure 7) of all samples, in both 1-Ir and 2-Ir routes, showed similarities to those of AgNP-assembled GO sheets [1, 59]. Moreover, comparing with bare GO [1], D and G peaks (at ~1350 and~1600 cm^{-1}) of GAT nanocomposites were slightly more turbulent, indicating modifications in their structure. Raman spectra of gamma-irradiated GO and other graphene-based materials (rGO, GONR, and rGONR) obtained in previous publications such as that of

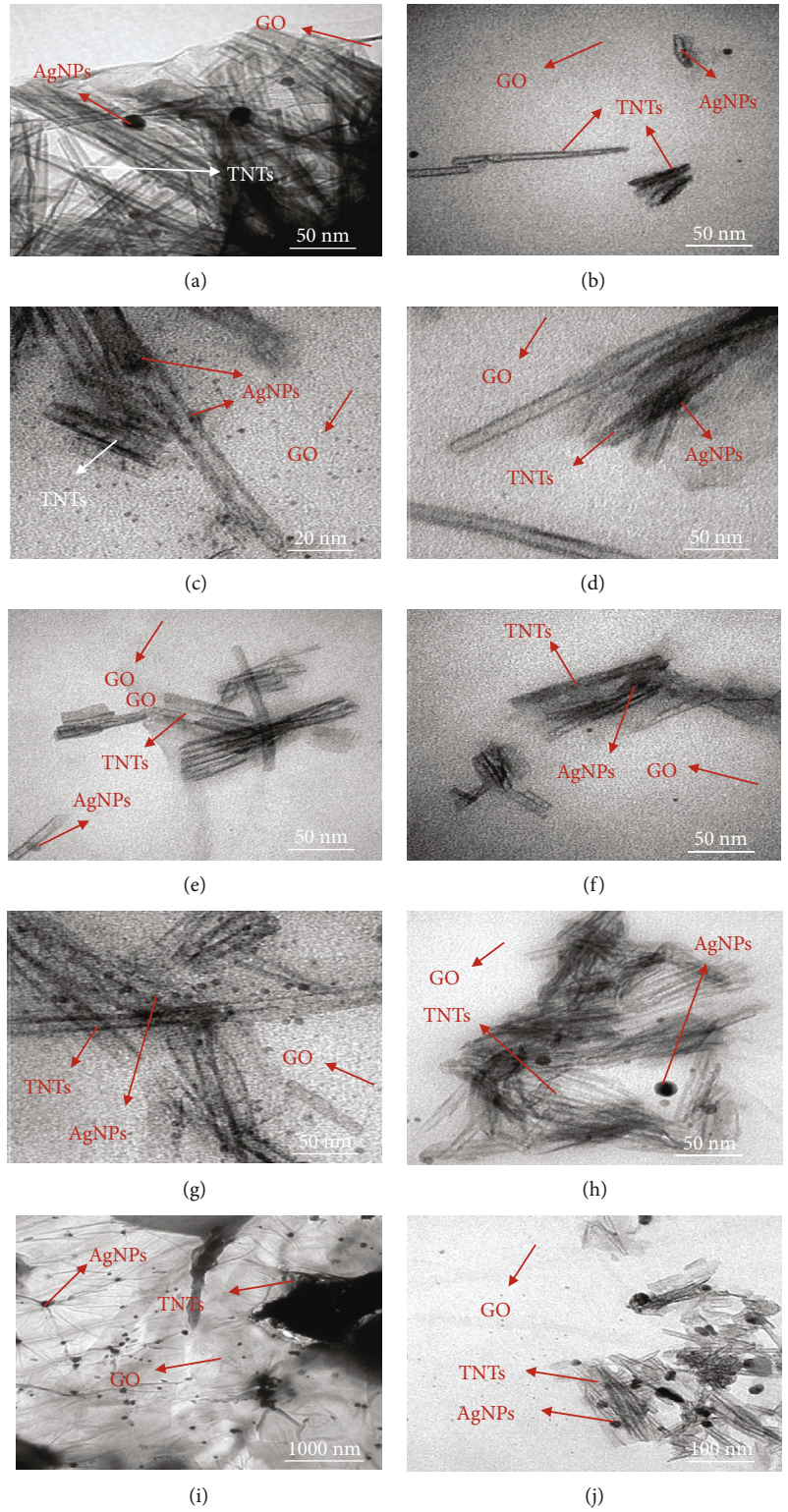

Figure 10: TEM images of 1-Ir route ((a–e) GAT-1-Ir-5 to GAT-1-Ir-25) and 2-Ir route ((f–j) GAT-2-Ir-5 to GAT-2-Ir-25) nanocomposites.

Vasilaki et al. [55] showed that after being irradiated, the G peak of GO became sharper and its ratio with the D peak increased as the irradiation dose augmented. Obtained Raman spectra of all GAT samples were the most similar to those of GO in Vasilaki et al.'s publication, indicating that GO was partially reduced during the exposure to gamma ray and the structure modification which resulted from the bonding with TiO_2 nanotubes and silver nanoparticles. TNTs' signal (B_{2g} peak at ~820 cm^{-1}) was slightly stronger in 2-Ir route samples than in 1-Ir route ones, indicating the

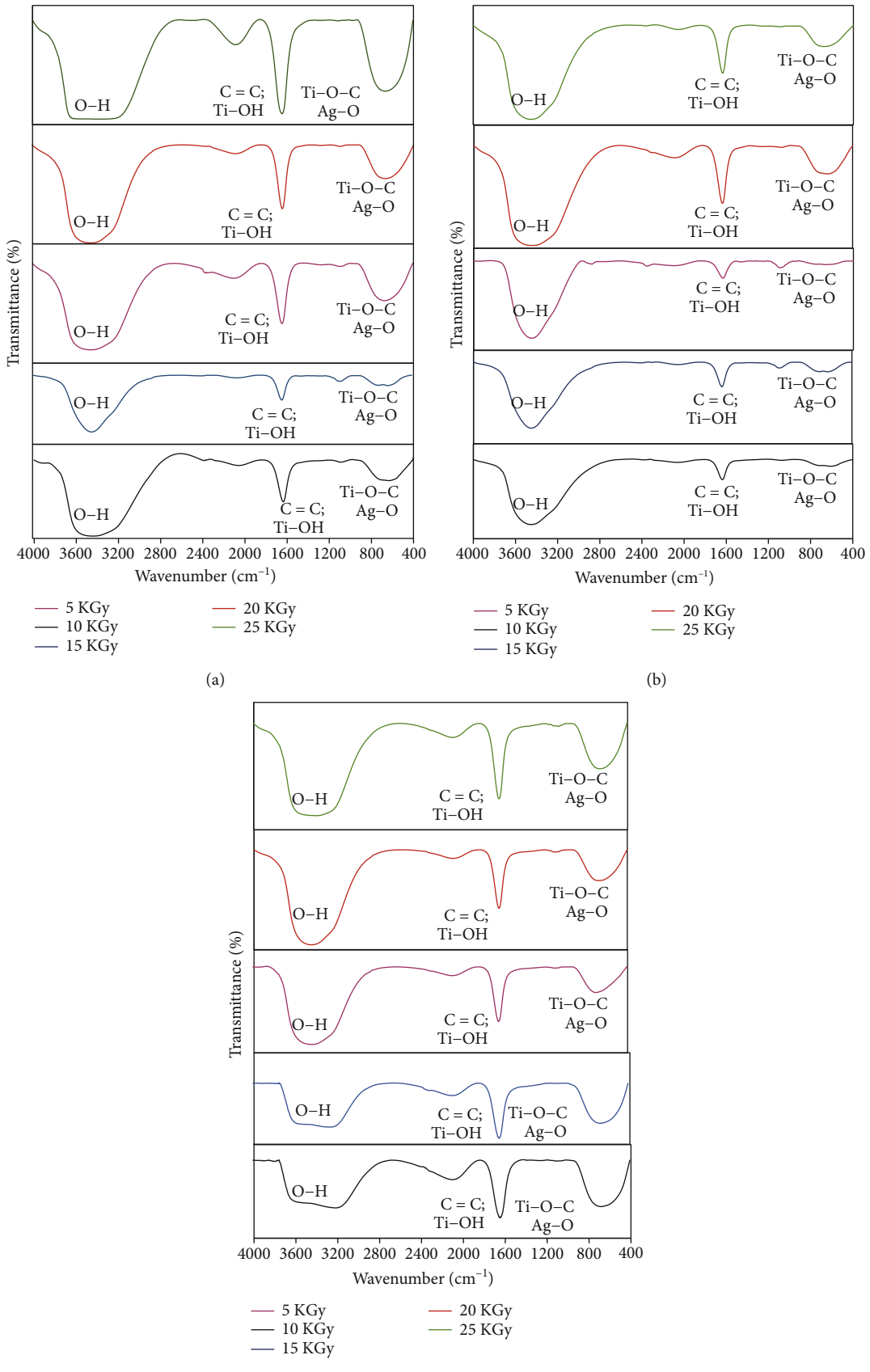

Figure 11: FT-IR spectra of nanocomposites irradiated without i-PrOH and N_2O (a), with i-PrOH (b), and with N_2O (c), at different doses.

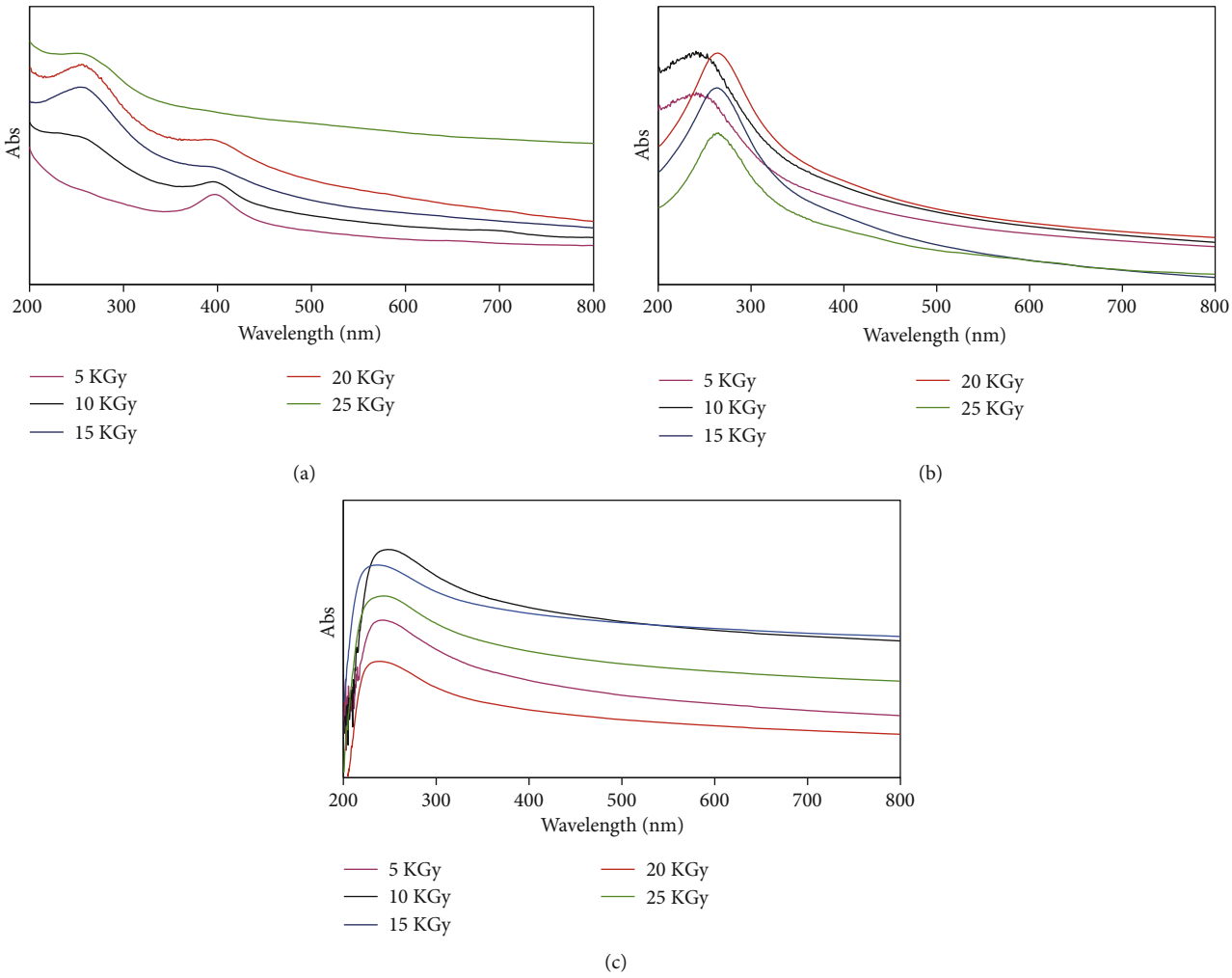

Figure 12: UV-Vis adsorption spectra of nanocomposites irradiated without i-PrOH and N_2O (a), with i-PrOH (b), and with N_2O (c), at different doses.

interaction between TNTs and AgNPs in the two-step gamma irradiation assistance.

XRD diffractograms (Figure 8) showed no obvious differences between 1-Ir route and 2-Ir route samples, and identical patterns of GO, TNTs, and AgNPs were not observed clearly. In addition, there were no obvious differences between the diffractograms GAT samples as the irradiation dose increased. By means of characterizing the FT-IR, UV-Vis absorption, and Raman spectroscopic data, GO, AgNPs, and TNTs were revealed to have interacted to form the GAT nanocomposite after the exposure to gamma ray. The possible cause of those XRD diffractogram observations, therefore, was the too low concentration of GAT nanocomposite in final solutions, which were taken directly to XRD diffractogram recording. Similar features were observed in other publications [60, 61].

Morphological properties of GAT nanocomposites, revealed by SEM and TEM images (Figures 9 and 10), corresponded well with our previous considerations. As the irradiation doses and times increased, only TNT component could be observed with clearest shape. In addition, silver nanoparticles showed the tendency of agglomerating, hence

Table 1: Proportion of GO, AgNPs, and TNTs (%) of GAT nanocomposites.

Sample	GO (%)	AgNPs (%)	TNTs (%)
GAT-1-Ir-5	67.11 ± 0.02	$0.002E^{-4}$ ± 0.03	31.78 ± 0.02
GAT-1-Ir-10	69.33 ± 0.01	5.11 ± 0.02	26.04 ± 0.01
GAT-1-Ir-15	72.60 ± 0.02	$0.009E^{-4}$ ± 0.02	26.88 ± 0.02
GAT-1-Ir-20	64.91 ± 0.01	$0.009E^{-4}$ ± 0.01	34.98 ± 0.01
GAT-1-Ir-25	89.01 ± 0.02	$0.001E^{-4}$ ± 0.01	10.87 ± 0.01

Table 2: Decoloration efficiency (DE, %) of GAT nanocomposites.

Sample	C_0 (ppm)	Abs	C (ppm)	DE (%)
GAT-1-Ir-5	10	1.44 ± 0.01	6.83 ± 0.01	31.69 ± 0.02
GAT-1-Ir-10	10	0.40 ± 0.01	1.88 ± 0.01	81.21 ± 0.02
GAT-1-Ir-15	10	1.50 ± 0.02	7.14 ± 0.02	28.55 ± 0.03
GAT-1-Ir-20	10	1.33 ± 0.01	6.31 ± 0.01	36.88 ± 0.03
GAT-1-Ir-25	10	0.82 ± 0.01	3.88 ± 0.01	61.17 ± 0.02

Table 3: Measurement parameters and RhB decoloration efficiency (DE, %) of the 10 kGy GAT, bare components and other related materials.

Sample	Amount of materials (mg)	Amount of RhB (mL of 10 ppm solution)	Photodegradation duration (min)	DE (%)	Ref.
GAT-1-Ir-10	0.3	20	60	81.21	—
GO	0.27	20	60	22.25	Thuy et al.
AgNPs	0.02	20	60	1.52	Thuy et al.
TNTs	0.10	20	60	10.58	Thuy et al.
P25	100	200	60	81.8	Guo et al.
TiO_2 nanowires	100	200	60	91.9	Guo et al.

their increase in diameter. All images also showed that in the GAT nanocomposites, both TiO_2 nanotubes and silver nanoparticles were assembled on the surface of GO, as well as the embellishment of silver nanoparticles on TiO_2 nanotubes. During two-time exposure to gamma ray, TiO_2 nanotubes increased in crystallization, and silver nanoparticles exhibited the trend of assembling directly on GO's surface.

3.1.2. Effect of the Presence of Isopropanol (I-PrOH) and Nitrous Oxide (N_2O). Obtained results regarding the gamma ray irradiation assistance steps on GAT nanocomposite led to our consideration that two steps of assistance exhibited certain effects on some of the chemical bonds among GO, AgNPs, and TNTs. Due to such influence, investigation on the effects of gamma ray on GAT nanocomposite with i-PrOH and N_2O's presence could be complicated and inaccurate. Therefore, only the 1-Ir route samples were investigated. The FT-IR spectra (Figure 11) showed differences in the samples irradiated with the presence of i-PrOH and N_2O. Specifically, with the presence of i-PrOH, signals of Ti – OH bond (at ~1620 cm^{-1}); Ti – O – C and Ag – O bonds (at ~500-700 cm^{-1}) were weaker, indicating fewer bonds formed, in comparison with non-i-PrOH samples. As the irradiation dose increased, those signals became stronger. It can be inferred from these results that the release of free radicals (·OH) during the irradiation played an important role for the bonding among GO, AgNPs, and TNTs. Due to the i-PrOH's radical scavenging ability, GO, AgNPs, and TNTs were not as well bonded as in the non-i-PrOH case. For the N_2O case, the signals were almost as strong as the non-N_2O samples. As the irradiation dose increased, the signals became stronger, but the change was not as much as the i-PrOH case. This result could be explained based on the radiolysis reaction of water in GAT solutions under gamma ray exposure (Figure 1), which releases hydrated electrons. These electrons were captured by N_2O, hence the favorability of releasing more electrons and radicals [62]. Being a gas, the contact surface of N_2O with the GAT solution was lower than that of i-PrOH, hence its lower effect on GAT nanocomposite during exposure to gamma ray irradiation. All obtained results led to our consideration that the gamma ray irradiation released free radicals and hydrated electrons, which played an important role for the bonding of GO, AgNPs, and TNTs in the nanocomposite.

UV-Vis absorption spectra (Figure 12) showed significant differences in the GAT nanocomposites irradiated with the presence of i-PrOH and N_2O. For details, in the "i-PrOH samples", AgNPs' signal (at ~400 nm) became stronger, and then weaker as the irradiation dose increased, while that of TNTs (at ~270 nm) only became stronger. As a radical capturer, i-PrOH decreased the number of radicals in the solutions, of which consequence was the diminution of reactive moieties for AgNPs formation. Secondly, the capability of capturing radicals of i-PrOH prevents partially structure defects of TiO_2 under gamma ray irradiation. Similar explanations were reported in previous publications [63]. In the case of N_2O, only the signal of TNTs was obvious, of which possible cause was the hydrated electron scavenging of N_2O. The absence of hydrated electrons led to the prevention of denaturalization of linked components in GAT nanocomposite. The spectra of all samples resembled those of nanocomposites, with stable bonds between constituents [64].

All obtained results resulted in our consideration that the variation of gamma irradiation dose and assistance caused certain effects on the characteristics of GAT nanocomposite in the tendency of bonding GO, AgNPs, and TNTs, while the presence of isopropanol and N_2O assured the release of radicals and electrons from these components during the exposure to gamma ray, which played an important role in their interaction.

3.2. GAT Nanocomposites' Rhodamine B Photodecomposition. Due to the structure denaturalization of 2-Ir route samples under numerous times of irradiation, which was discussed profoundly in previous sections, their ability of photodecomposing RhB would certainly be affected. Therefore, only 1-Ir route samples were followed by the proportion determination and the RhB photodegrading investigation. The proportion of GO, AgNPs, and TNTs in GAT nanocomposites were shown in Table 1.

UV-Vis absorption evaluation for RhB's 10 ppm solution and standard curve led to its determined maximum adsorption peak at ~553.5 nm and recurrent equation as $y = 0.2092x + 0.0086$ ($R^2 = 0.9997$). The decoloration efficiency, or DE, values of GAT nanocomposites were shown in Table 2.

It was obvious in Table 2 that the sample with irradiation dose of 10 kGy exhibited the highest photodecomposing activity, followed by the 25 kGy. This result was explained that at low irradiation dose, the agglomeration of silver nanoparticles, as well as the possibility of bond breaking, did not occur, hence the good photodecomposing activity. When the irradiation dose increased, silver nanoparticles coagulated, hence the diminution in RhB photodegrading ability. The increase in the photodegrading activity of the GAT

nanocomposite as the dose increased from 15 to 25 kGy could be explained by the higher crystallization of the TiO_2 component. Comparison with the photodecomposition ability of bare GO, TNTs, and AgNPs [1] and related publication [65], the 10 kGy sample exhibited high photodegrading activity (Table 3).

4. Conclusion

In this work, effects of gamma ray irradiation conditions, including irradiation doses and steps of assistance, on the combination of GO, AgNPs, and TNTs were investigated, with the presence of i-PrOH and N_2O. It was revealed that gamma ray irradiation exhibited bonding effect, by means of releasing hydrated electrons and radicals. When the exposure to gamma ray was long enough, it exhibited certain effects on the formed chemical bonds among GO, AgNPs, and TNTs. One step of irradiation assistance, and at the low dose (10 kGy), was determined to be appropriate for the GAT formation. The nanocomposites showed good activity on RhB dye photodecomposing. As a simple and controllable manner, gamma ray irradiation showed high potential for applying in the synthesis of "tertiary" hybrid materials, as well as many other nanomaterials.

Data Availability

All of our research data regarding this study are accessible on the data repository of http://www.re3data.org/, which authors can search by means of the DataCite Repository Finder.

Conflicts of Interest

All of the authors declare that no potential conflicts of interest could be perceived to affect the objectivity or neutrality of this article.

Acknowledgments

This research is funded by the Vietnam National Foundation for Science and Technology Development (NAFOSTED) under Grant Number 104.03-2017.49.

References

[1] T. L. P. Thi, D. K. N. Vu, P. A. N. Thi, and D. K. V. Nguyen, "Silver nanoparticles-assembled graphene oxide sheets on TiO_2 nanotubes: synthesis, characterization, and photocatalytic investigation," *Applied Nanoscience*, vol. 10, no. 10, pp. 3735–3743, 2020.

[2] G. G. Flores-Rojas, F. López-Saucedo, and E. Bucio, "Gamma-irradiation applied in the synthesis of metallic and organic nanoparticles: a short review," *Radiation Physics and Chemistry*, vol. 169, pp. 1–46, 2018.

[3] A. I. El-Batal, M. S. Nagwa, A. A. Ismail, A. A. Rawia, and M. F. Rasha, "Impact of silver and selenium nanoparticles synthesized by gamma irradiation and their physiological response on early blight disease of potato," *Journal of Chemical and Pharmaceutical Research*, vol. 8, pp. 934–951, 2016.

[4] D. N. V. Khoa, K. Christelle, D. Laurent, C. Xavier, and Q. H. Nguyen, "Radiation synthesis of chitosan stabilized gold nanoparticles comparison between e^- beam and γ irradiation," *Radiation Physics and Chemistry*, vol. 94, pp. 1–4, 2014.

[5] T. Yousefi and H. R. Moazami, "Water radiolysis by gamma – irradiation for high quality synthesis of nickel oxide nano sheet," *Journal of Nanostructures*, vol. 9, pp. 141–145, 2019.

[6] C. J. Lee, M. R. Karim, T. Vasudevan et al., "A comparison method of silver nanoparticles prepared by the gamma irradiation and *in situ* reduction methods," *Bulletin of the Korean Chemical Society*, vol. 31, no. 7, pp. 1993–1996, 2010.

[7] X. Chen, M. Qiu, S. Li et al., "Gamma-ray irradiation to accelerate crystallization of mesoporous zeolites," *Angewandte Chemie, International Edition*, vol. 59, no. 28, pp. 1325–11329, 2020.

[8] D. Ding, D. Zhang, F. He, G. Xie, and X. Chen, "Gamma-ray irradiation effects on tantalum thin film for improved mechanical compatibility and cytocompatibility," *Materials Science and Engineering: C*, vol. 110, p. 110700, 2020.

[9] A. K. Anbalagan, C. Jao, M. Syabriyana et al., "Influence of gamma-ray irradiation and post-annealing studies on pentacene films: the anisotropic effects on structural and electronic properties," *RSC Advances*, vol. 10, no. 36, pp. 21092–21099, 2020.

[10] H. J. L. Junior, C. A. Duarte, M. W. S. Pinto, W. D. Foryta, B. G. Titon, and E. M. G. Vasconcellos, "Influence of gamma ray irradiation on the optical properties of calcite and dolomite," *Applied Spectroscopy*, vol. 74, no. 5, pp. 507–514, 2020.

[11] Y. Shin, J. Choi, J. Na, and S. Y. Kim, "Thermally triggered soft actuators based on a bilayer hydrogel synthesized by gamma ray irradiation," *Polymer*, vol. 212, article 123163, 2020.

[12] C. Liu, J. Zhang, W. Wang, Y. Guo, and K. Xiao, "Effects of gamma-ray irradiation on separation and mechanical properties of polyamide reverse osmosis membrane," *Journal of Membrane Science*, vol. 611, p. 118354, 2020.

[13] A. K. Anbalagan, S. Gupta, A. kumar et al., "Gamma ray irradiation enhances the linkage of cotton fabrics coated with ZnO nanoparticles," *ACS Omega*, vol. 5, no. 25, pp. 15129–15135, 2020.

[14] G. Yang, N. Song, F. Deng et al., "Direct surface functionalization of graphene oxide with ionic liquid through gamma ray irradiation induced radical polymerization with remarkable enhanced adsorption capacity," *Journal of Molecular Liquids*, vol. 306, p. 112877, 2020.

[15] L. M. F. Batista, V. K. Meader, K. V. Romero et al., "Kinetic control of $[AuCl_4]^-$ photochemical reduction and gold nanoparticle size with hydroxyl radical scavengers," *The Journal of Physical Chemistry. B*, vol. 133, pp. 7204–7213, 2019.

[16] J. S. Choi, J. Sohn, and J. Shin, "A comparative study on EB-radiation deterioration of nafion membrane in water and isopropanol solvents," *Energies*, vol. 8, no. 6, pp. 5370–5380, 2015.

[17] S. Sato, R. Yugeta, K. Shinsaka, and T. Terao, "Nitrous oxide as an electron scavenger in the radiolysis of hydrocarbons," *Bulletin of the Chemical Society of Japan*, vol. 39, no. 1, pp. 156–160, 1966.

[18] P. Das, B. Rout, U. Manju, and S. Chatterjee, "Tunable wettability and conductivity of graphene oxide surface with insights from density functional theory and molecular dynamics investigations," *Journal of Physical Chemistry C*, vol. 124, no. 19, pp. 10541–10549, 2020.

[19] Y. Cui, S. Kundalwal, and S. Kumar, "Gas barrier performance of graphene/polymer nanocomposites," *Carbon*, vol. 98, pp. 313–333, 2016.

[20] A. T. Smith, A. M. LaChance, S. Zeng, B. Liu, and L. Sun, "Synthesis, properties, and applications of graphene oxide/reduced graphene oxide and their nanocomposites," *Nano Materials Science*, vol. 1, pp. 31–47, 2019.

[21] S. Pakapongpan, A. Tuantranont, and R. P. Poo-arporn, "Magnetic nanoparticle-reduced graphene oxide nanocomposite as a novel bioelectrode for mediatorless-membraneless glucose enzymatic biofuel cells," *Scientific Reports*, vol. 7, pp. 1–12, 2017.

[22] T. S. Anirudhan and S. M. Anju, "Synthesis and evaluation of TiO_2 nano-tubes/silylated graphene oxide-based molecularly imprinted polymer for the selective adsorption and subsequent photocatalytic degradation of 2,4-dichlorophenoxyacetic acid," *Journal of Environmental Chemical Engineering*, vol. 7, no. 5, p. 103355, 2019.

[23] M. Wei, J. Wan, Z. Hu, Z. Peng, and B. Wang, "Enhanced photocatalytic degradation activity over $_{TiO\ 2}$ nanotubes co-sensitized by reduced graphene oxide and copper(II) meso -tetra(4-carboxyphenyl)porphyrin," *Applied Surface Science*, vol. 377, pp. 149–158, 2016.

[24] D. Beketova, M. Motola, H. Sopha et al., "One-step decoration of TiO_2 nanotubes with Fe_3O_4 nanoparticles: synthesis and photocatalytic and magnetic properties," *ACS Applied Nano Materials*, vol. 3, no. 2, pp. 1553–1563, 2020.

[25] M. Safavipour, M. Kharaziha, E. Amjahi, F. Karimzadeh, and A. Allafchian, "TiO_2 nanotubes/reduced GO nanoparticles for sensitive detection of breast cancer cells and photothermal performance," *Talanta*, vol. 208, p. 120369, 2020.

[26] L. A. Al-Haiji, A. A. Ismail, A. Al-Hazza et al., "Impact of calcination of hydrothermally synthesized TiO_2 nanowires on their photocatalytic efficiency," *Journal of Molecular Structure*, vol. 1200, p. 127153, 2020.

[27] V. Galstyan, A. Ponzoni, I. Kholmanov, M. M. Natile, E. Cornini, and G. Sberveglieri, "Highly sensitive and selective detection of dimethylamine through Nb-doping of TiO_2 nanotubes for potential use in seafood quality control," *Sensors and Actuators B: Chemical*, vol. 303, p. 127217, 2020.

[28] N. Khaliq, M. A. Rasheed, G. Cha et al., "Development of non-enzymatic cholesterol bio-sensor based on TiO_2 nanotubes decorated with Cu_2O nanoparticles," *Sensors and Actuators B: Chemical*, vol. 302, p. 127200, 2020.

[29] M. H. Razali, N. A. Ismail, and K. A. M. Amin, "Titanium dioxide nanotubes incorporated gellan gum bio-nanocomposite film for wound healing: effect of TiO_2 nanotubes concentration," *International Journal of Biological Macromolecules*, vol. 153, pp. 1117–1135, 2020.

[30] A. B. Tesler, M. Altomare, and P. Schmuki, "Morphology and optical properties of highly ordered TiO_2 nanotubes grown in NH_4F/*o*-H_3PO_4 electrolytes in view of light-harvesting and catalytic applications," *ACS Applied Nano Materials*, vol. 3, no. 11, pp. 10646–10658, 2020.

[31] X. Xie, L. Li, S. Ye, Q. Zhang, X. Chen, and X. Huang, "Photocatalytic degradation of ethylene by TiO_2 nanotubes/ reduced graphene oxide prepared by gamma irradiation," *Radiation Physics and Chemistry*, vol. 165, p. 108371, 2019.

[32] Q. Zhang, S. Ye, X. Song, and S. Luo, "Photocatalyst based on TiO_2 nanotube arrays co-decorated with CdS quantum dots and reduced graphene oxide irradiated by γ rays for effective degradation of ethylene," *Applied Surface Science*, vol. 442, pp. 245–255, 2018.

[33] T. C. Mesquita, M. C. E. V. Schiassi, A. M. T. Lago et al., "Grape juice blends treated with gamma irradiation evaluated during storage," *Radiation Physics and Chemistry*, vol. 168, p. 108570, 2020.

[34] Q. Zhao, R. Goto, T. Saito, T. Kobayashi, and T. Sasaki, "Effect of gamma-irradiation on complexation of humic substances with divalent calcium ion," *Chemosphere*, vol. 256, p. 127021, 2020.

[35] A. Ganguli, P. Ganguly, P. Das, and A. Saha, "Integral approach for the treatment of phenolic wastewater using gamma irradiation and graphene oxide," *Groundwater for Sustainable Development*, vol. 10, p. 10355, 2020.

[36] S. Wang, W. Wang, L. Yue et al., "Hierarchical Cu_2O nanowires covered by silver nanoparticles-doped carbon layer supported on Cu foam for rapid and efficient water disinfection with lower voltage," *Chemical Engineering Journal*, vol. 382, p. 122855, 2020.

[37] W. Zhang, X. Wang, Y. Zhang et al., "Robust shape-retaining nanocellulose-based aerogels decorated with silver nanoparticles for fast continuous catalytic discoloration of organic dyes," *Separation and Purification Technology*, vol. 242, p. 116523, 2020.

[38] G. Tang, F. Su, X. Xu, and P. K. Chu, "2D black phosphorus dotted with silver nanoparticles: an excellent lubricant additive for tribological applications," *Chemical Engineering Journal*, vol. 392, p. 123631, 2020.

[39] X. Hu, Y. Hu, G. Xu et al., "Green synthesis of a magnetic β-cyclodextrin polymer for rapid removal of organic micropollutants and heavy metals from dyeing wastewater," *Environmental Research*, vol. 180, p. 108796, 2020.

[40] H. K. Leong, P. C. Sim, D. Bahnemann, M. Jang, S. Ibrahim, and P. Saravanan, "Reduced graphene oxide and Ag wrapped TiO_2 photocatalyst for enhanced visible light photocatalysis," *APL Materials*, vol. 3, no. 10, p. 104503, 2015.

[41] Q. Zhou, M. Wang, Y. Tong et al., "Improved photoelectrocatalytic degradation of tetrabromobisphenol a with silver and reduced graphene oxide-modified TiO_2 nanotube arrays under simulated sunlight," *Ecotoxicology and Environmental Safety*, vol. 182, p. 109472, 2019.

[42] M. Faraji and N. Mohaghegh, "Ag/TiO_2-nanotube plates coated with reduced graphene oxide as photocatalysts," *Surface and Coating Technology*, vol. 288, pp. 144–150, 2016.

[43] D. C. Marcano, D. V. Kosynkin, J. M. Berlin et al., "Improved synthesis of graphene oxide," *ACS Nano*, vol. 4, no. 8, pp. 4806–4814, 2010.

[44] D. Aherne, D. M. Ledwith, M. Gara, and J. M. Kelly, "Optical properties and growth aspects of silver nanoprisms produced by a highly reproducible and rapid synthesis at room temperature," *Advanced Functional Materials*, vol. 18, no. 14, pp. 2005–2016, 2008.

[45] M. A. L. Zavala and M. Ávila-Santos, "Synthesis of stable TiO_2 nanotubes: effect of hydrothermal treatment, acid washing and annealing temperature," *Heliyon*, vol. 3, no. 11, article e00456, 2017.

[46] A. Kumar, A. Mahajan, and Z. Begum, "Phytochemical screening and *in vitro* study of free radical scavenging activity of flavonoids *of aloe vera*," *Research Journal of Pharmacy and Technology*, vol. 13, no. 2, pp. 593–598, 2020.

[47] J. Zhang, L. Zheng, F. Wang et al., "The critical role of furfural alcohol in photocatalytic H_2O_2 production on TiO_2," *Applied Catalysis B: Environmental*, vol. 269, p. 118770, 2020.

[48] R. Nagaraja, N. Kottam, C. R. Girija, and B. M. Nagabhushana, "Photocatalytic degradation of Rhodamine B dye under UV/solar light using ZnO nanopowder synthetized by solution combustion route," *Powder Technology*, vol. 215, pp. 91–97, 2012.

[49] A. León, P. Reuquen, C. Garín et al., "FTIR and Raman characterization of TiO_2 nanoparticles coated with polyethylene glycol as carrier for 2-methoxyestradiol," *Applied Sciences*, vol. 7, pp. 1–9, 2017.

[50] W. Li, B. Song, S. Zhang et al., "Using 3-isocyanatopropyltrimethoxysilane to decorate graphene oxide with nano-titanium dioxide for enhancing the anti-corrosion properties of epoxy coating," *Polymers*, vol. 12, no. 4, p. 837, 2020.

[51] D. V. N. Khang and D. N. V. Khoa, "Magnetite nanoparticles-TiO_2 nanoparticles-graphene oxide nanocomposite: synthesis, characterization and photocatalytic degradation for Rhodamine-B dye," *AIMS Materials Science*, vol. 7, pp. 288–301, 2020.

[52] T. F. Emiru and D. W. Ayele, "Controlled synthesis, characterization and reduction of graphene oxide: a convenient method for large scale production," *Egyptian Journal of Basic and Applied Sciences*, vol. 4, pp. 74–79, 2017.

[53] L. Wang, B. Chen, J. Ma, G. Cui, and L. Chen, "Reviving lithium cobalt oxide-based lithium secondary batteries toward a higher energy density," *Chemical Society Reviews*, vol. 47, no. 17, pp. 6505–6602, 2018.

[54] O. I. Shpotyuk, M. M. Vakiv, M. V. Shpotyuk, and S. A. Kozyukhin, "Metallic nanoparticles (Cu, Ag, Au) in chalcogenide and oxide glassy matrices: comparative assessment in terms of chemical bonding," *Semiconductor Physics Quantum Electronics & Optoelectronics*, vol. 20, no. 1, pp. 26–33, 2017.

[55] E. Vasilaki, I. Georgaki, D. Vernardou, M. Vamvakaki, and N. Katsarakis, "Ag-loaded TiO_2/reduced graphene oxide nanocomposites for enhanced visible-light photocatalytic activity," *Applied Surface Science*, vol. 353, pp. 865–872, 2015.

[56] A. Ansón-Casaos, J. A. Puértolas, F. J. Pascual et al., "The effect of gamma-irradiation on few-layered graphene materials," *Applied Surface Science*, vol. 301, pp. 264–272, 2014.

[57] P. Chen, L. Song, Y. Liu, and Y. Fang, "Synthesis of silver nanoparticles by γ-ray irradiation in acetic water solution containing chitosan," *Radiation Physics and Chemistry*, vol. 76, no. 7, pp. 1165–1168, 2007.

[58] Y. Li, L. Zhang, W. Wu, and G. Li, "Hydrothermal growth of TiO_2 nanowire membranes sensitized with CdS quantum dots for the enhancement of photocatalytic performance," *Nanoscale Research Letters*, vol. 9, no. 1, p. 270, 2014.

[59] Z. Li, S. Jiang, Y. Huo et al., "3D silver nanoparticles with multilayer graphene oxide as a spacer for surface enhanced Raman spectroscopy analysis," *Nanoscale*, vol. 10, no. 13, pp. 5897–5905, 2018.

[60] N. Supraja and T. Prasad, "synthesis, characterization and dose dependent antimicrobial and anti-cancerous activity of phycogenic silver nanoparticles against human hepatic carcinoma (HepG2) cell line," *AIMS Bioengineering*, vol. 3, no. 4, pp. 425–440, 2016.

[61] G. A. Otunola, A. J. Afolayan, E. O. Ajayi, and S. W. Odeyemi, "Characterization, antibacterial and antioxidant properties of silver nanoparticles synthesized from aqueous extracts of *Allium sativum*, *Zingiber officinale*, and *Capsicum frutescens*," *Pharmacognosy Magazine*, vol. 13, no. 50, pp. 201–208, 2017.

[62] S. Kongmany, M. Furuta, H. Matsuura, S. Okuda, K. Imamura, and Y. Maeda, "Degradation of phorbol 12,13-diacetate in aqueous solution by gamma irradiation," *Radiation Physics and Chemistry*, vol. 105, pp. 98–103, 2014.

[63] S. M. Hong, S. Lee, H. J. Jung et al., "Simple preparation of anatase TiO2Nanoparticles via pulsed laser ablation in liquid," *Bulletin of the Korean Chemical Society*, vol. 34, no. 1, pp. 279–282, 2013.

[64] M. Nasrollahzadeh, M. Atarod, B. Jaleh, and M. Gandomirouzbahani, "*In Situ* green synthesis of Ag nanoparticles on graphene oxide/TiO_2 nanocomposite and their catalytic activity for the reduction of 4-nitrophenol, Congo red and methylene blue," *Ceramics International*, vol. 42, no. 7, pp. 8587–8596, 2016.

[65] C. Guo, J. Xu, Y. He, Y. Zhang, and Y. Wang, "Photodegradation of Rhodamine B and methyl orange over one-dimensional TiO_2 catalysts under simulated solar irradiation," *Applied Surface Science*, vol. 257, no. 8, pp. 3798–3803, 2011.